ResearchGate

See discussions, stats, and author profiles for this publication at: https://www.researchgate.net/publication/230760538

Switching of Conductance in a Molecular Wire: Role of Junction Geometry, Interfacial Distance, and Conformational Change

ARTICLE *in* THE JOURNAL OF PHYSICAL CHEMISTRY C · JULY 2012

Impact Factor: 4.77 · DOI: 10.1021/jp3043335

CITATIONS
15

READS
31

3 AUTHORS, INCLUDING:

Kamal B. Dhungana
Michigan Technological University
8 PUBLICATIONS **26** CITATIONS

SEE PROFILE

Subhasish Mandal
Yale University
8 PUBLICATIONS **62** CITATIONS

SEE PROFILE

Available from: Kamal B. Dhungana
Retrieved on: 17 January 2016

THE JOURNAL OF PHYSICAL CHEMISTRY C

Article

pubs.acs.org/JPCC

Switching of Conductance in a Molecular Wire: Role of Junction Geometry, Interfacial Distance, and Conformational Change

Kamal B. Dhungana,[†] Subhasish Mandal,[†] and Ranjit Pati*,[†]

[†]Department of Physics, Michigan Technological University, Houghton, Michigan 49931, United States

ABSTRACT: Achieving atomic level control at the metal−molecule interface in a single molecule conductance measurement is a daunting challenge. An equally important issue is the lack of atomic level structural information of the interface, which makes the theoretical interpretation of observed conductance much harder; conductance sensitively depends upon the junction geometry. In this article, we report a junction dependent conductance study in a ruthenium−bis(terpyridine) molecular device, which has been fabricated and characterized (*J. Am. Chem. Soc.* **2008**, *130*, 2553) using a scanning tunneling microscope. An ensemble of device structures is created by varying metal−molecule binding sites, the orientation of the molecule at the interface, interfacial distances, and conformational change within the molecule to study junction dependent effects. An orbital dependent density functional theory in conjunction with a parameter free, single particle Green's function approach is used to study the current−voltage (I−V) characteristics. For the ONTOP junction geometry, our results show a sharp increase in current at a threshold voltage (V_{th}). The current is found to be relatively small (OFF state) for bias range below the threshold value. As we approach the weakly coupled regime, a drop in V_{th} is found; following a sharp increase in current at V_{th}, a current plateau (ON state) is observed with the increase of bias beyond $\sim V_{th}$. A similar nonlinear I−V curve with a current switching feature is reported by the experiment. An analysis of bias dependent transmission and orbital characters of participating eigen-channels is presented to understand the origin of distinct I−V features observed in strongly and weakly coupled junctions.

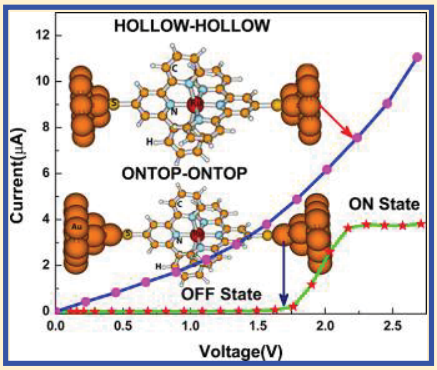

I. INTRODUCTION

The envisioning of a functional molecular device by Aviram and Ratner[1] and its subsequent realization by successfully connecting at least a single or a few molecules to a metal contact have opened up a new frontier in nanoscience research.[2−5] Researchers are relentlessly looking for molecules with rich chemistry to devise new devices with novel functionalities. Several groups have been successful in demonstrating conduction, rectification, and switching in molecular junctions; see refs 6 and 7 for a comprehensive review. However, the experimental difficulty of achieving robust atomic level control at the metal−molecule interface hinders the progress in this field. A statistical approach involving measurement of conductance by repeatedly forming thousands of metal−molecule junctions has been used by researchers to extract reliable data for the conductance in the molecular junction.[8−10] Yet, the qualitative as well as quantitative interpretations of experimental data pose a significant challenge, as the atomic level structural details of the junctions are not available *a priori*. In addition, the conformation of the molecule as well as the contact structure, which evolve dynamically during experimental measurements, make the theoretical task much harder. Thus, a true understanding of experimental data can only be achieved by a theoretical calculation of conductance in an ensemble of molecular wires with different junction geometries.[11−14]

In this article, we investigate the junction dependent current−voltage characteristics in a molecular junction consisting of the ruthenium−bis(terpyridine) interconnect attached between two gold electrodes. The thiolate (-S) group is used to anchor the molecule to the gold (111) electrode; the most likely ONTOP and HOLLOW binding sites are considered. The ONTOP binding site refers to the junction geometry, where the S atom is directly on the top of the Au atom. For the HOLLOW binding site, the S atom is on the 3-fold hollow site of the Au(111) surface.[15] The ruthenium−bis(terpyridine) junction is of interest because it has been fabricated and the electron transport property has been measured[16] using scanning tunneling microscopy (STM). By sweeping the tip bias from 0 to 2 V, a sudden increase in current is reported at a threshold tip bias (V_{th}) of ∼1.7 V. The current is reported to be small and remains flat (OFF state) for the bias range below the threshold value. When the tip-bias is increased beyond V_{th}, a current plateau is observed (ON state).[16] Despite this experimental observation, only nominal theoretical efforts are made to identify the origin of such switching behavior in the current. There are several unanswered questions: What causes the current to increase sharply at a threshold bias? Which junction geometry is likely to yield such a nonlinear I−V curve? What is the role of conformational change within the molecule? We answer these subtle questions in this article.

Received: May 4, 2012
Revised: July 17, 2012
Published: July 19, 2012

 © 2012 American Chemical Society

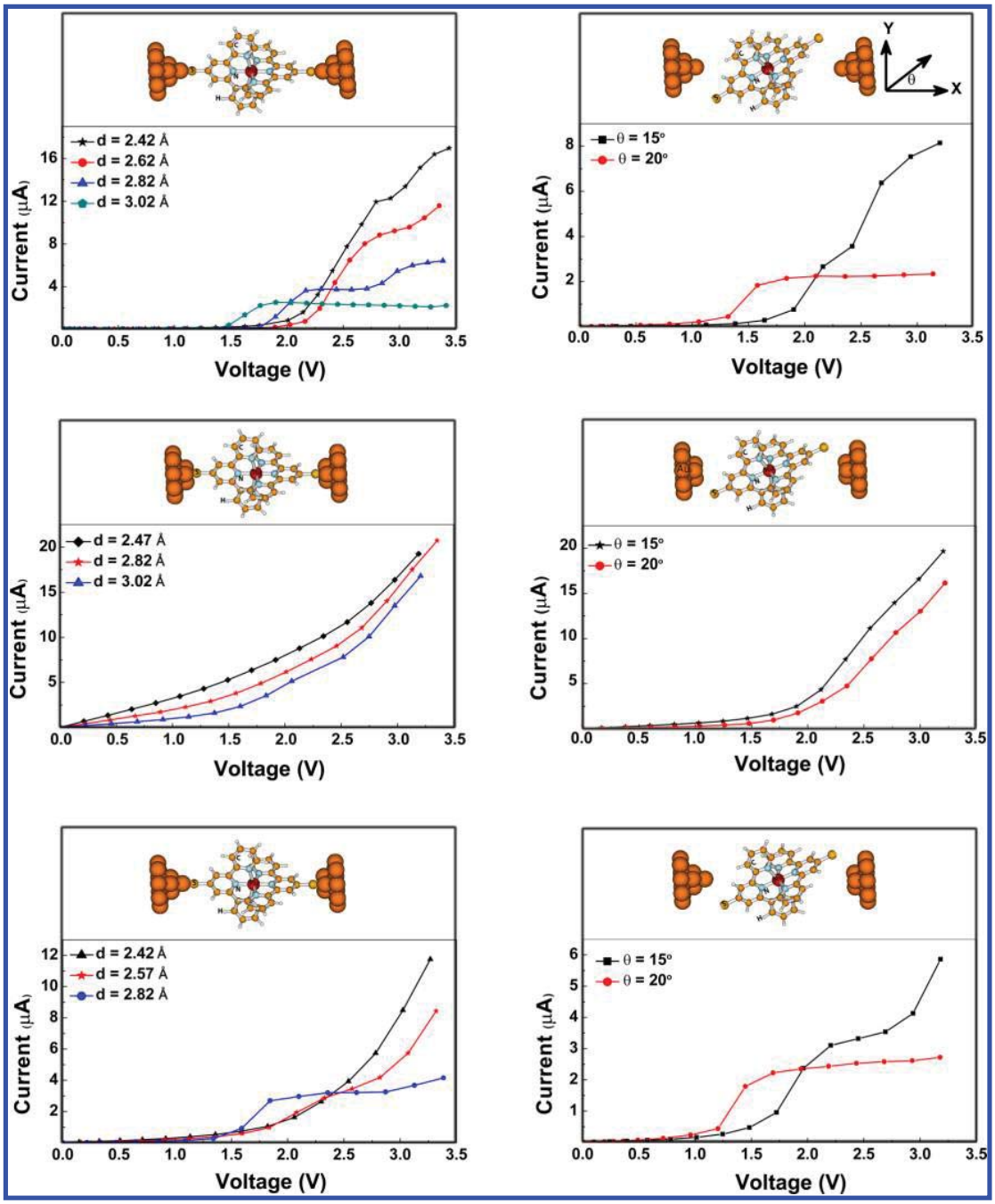

Figure 1. Calculated current (I)−voltage (V) characteristics for Ru−bis(terpyridine) molecular wires with different junction configurations. Top and bottom panels show the junction structure and the corresponding $I-V$ characteristic, respectively. Junction geometries: (a) ONTOP−ONTOP at both interfaces; (b) ONTOP−ONTOP at both interfaces with the molecular spacer rotated by an angle θ about the Z axis; (c) HOLLOW−HOLLOW at both interfaces; (d) HOLLOW−HOLLOW at both interfaces with the molecular spacer rotated by an angle θ about the Z axis; (e) ONTOP−HOLLOW at two interfaces; (f) ONTOP−HOLLOW at two interfaces with the molecular spacer rotated by an angle θ about the Z axis. The distance d refers to the interplanar distance between the sulfur and the nearest gold; the X axis represents the direction of current flow.

We have built numerous prototypical molecular junctions by varying junction geometries, S−Au interfacial distance, orientation angle at the junction, and conformational change within the molecule. A single particle Green's function formalism[11,17−27] in conjunction with the explicit orbital dependent density functional method (DFT)[28] involving the B3LYP[29,30] hybrid functional is used to calculate the electronic current in the molecular junction. Our calculation reveals a sensitive dependence of the $I-V$ feature on the junction geometry. For the ONTOP junction geometry, a sharp increase in current after a threshold bias is observed. Conformational change within the molecule is found to have no effect on V_{th}. As we approach the weakly coupled regime by increasing the interfacial distance, the value for V_{th} is found to decrease and a current plateau is observed for bias beyond V_{th}; the plateau length is found to increase with the increase in interfacial distance(d). A similar feature in $I-V$ is reported by the STM experiment.[16] We look into the bias dependent transmission

dx.doi.org/10.1021/jp3043335 | J. Phys. Chem. C 2012, 116, 17268−17273

and orbital characters of the participating eigen-channels to identify the origin of the distinct features observed in the $I-V$ curve.

The rest of the paper is organized as follows. In section II, we present briefly the computational procedure. Results and discussions are described in section III followed by a brief summary in section IV.

II. COMPUTATIONAL METHODS

Our results are based on first principles DFT[28] calculations, which involve Becke's three-parameter hybrid functional (B3LYP)[29,30] for exchange and correlation. The use of the explicit orbital dependent B3LYP functional allows us to include a part of the exact Hartree−Fock exchange and thus corrects partly the self-interaction error. This self-interaction corrected scheme[13,21,26] has been reported to yield a lower current value that is found to be in better agreement with the experimentally measured current when compared with the calculated current obtained using other functionals (SVWN, PW91PW91, PW91LYP).[26] A real-space approach that employs the single determinant wave function is used here. A finite set of Gaussian atomic orbitals[29] is used to construct the trial wave function. To ensure a tight convergence during the self-consistent calculation, we have used the convergence thresholds for energy, maximum, and root-mean-square electron density as 10^{-6}, 10^{-6}, and 10^{-8} a.u., respectively. The all electron 6-311G* Gaussian basis set[29] is used to describe all the atoms in the thiolate terminated ruthenium−bis(terpyridine) complex except the Ru atom. For the gold atoms in the electrodes and the Ru atom in the molecule, we have used the LANL2DZ pseudopotential basis set[29] that includes the scalar relativistic effect.

The prototypical two-terminal molecular device is built by sandwiching the ruthenium−bis(terpyridine) complex between two semi-infinite gold electrodes; thiolate (-S) anchoring groups are used to attach the molecule between the electrodes. The optimized structure for the Ru−terpyridine complex in which the Ru atom is bonded to two terpyridine molecules in an approximate octahedral geometry is used to build the prototype. This open device has two parts. One part consists of the molecule and a finite number of gold atoms (taken from the Au (111) surface on both sides). This is called the active-scattering region. For the ONTOP configuration, we have included four gold atoms on each side, and for the HOLLOW configuration, we have included three gold atoms on each side in the active-scattering region. The other part is the semi-infinite part of the gold electrodes assumed to retain its bulk properties. We have used a single particle bias-dependent Green's function approach.[11,17−27] This approach allows us to convert the problem of the complicated experimental device into a problem of the active region, which is open to the electrodes through the self-energy functions ($\sum_{l,r}$). The bias-dependent Green's function of the device is calculated as[20,26,27]

$$G(E, \varepsilon) = [E \times S - H_{mol}(\varepsilon) - \sum_l(\varepsilon) - \sum_r(\varepsilon)]^{-1} \quad (1)$$

where H_{mol} is the bias-dependent Kohn−Sham molecular Hamiltonian obtained by suitable partitioning of $H(\varepsilon)$. The use of the real-space approach for the active scattering region allows us to partition the $H(\varepsilon)$ to obtain $H_{mol}(\varepsilon)$. E is the injection energy of the tunneling electron, and S is the molecular overlap matrix. The current is calculated using the multichannel Landuar−Buttiker formula,[17] given by

$$I = \frac{2e}{h}\int_{\mu_1}^{\mu_2} T(E, V) \times [f(E, \mu_2) - f(E, \mu_1)]\, dE \quad (2)$$

$T(E,V)$ is the bias dependent transmission function, calculated as[17,20,26,27]

$$T(E, V) = Tr(\Gamma_l G \Gamma_r G^{\dagger}) \quad (3)$$

where $\Gamma_{l,r} = i(\sum_{l,r} - \sum_{l,r}^{\dagger})$ is the broadening function that determines the escape rate of the electron. In eq 2, e is the electronic charge, h is Planck's constant, and f is the Fermi distribution function. The chemical potentials, $\mu_{1,2}$, are calculated as

$$\mu_{1,2} = E_f \mp V_{low,high} \quad (4)$$

E_f is the equilibrium Fermi energy; V_{low} and V_{high} are the voltage drops at the electrodes, which are calculated self-consistently.[26,27] The potential difference, V, is obtained from the difference of V_{low} and V_{high}; at equilibrium $V_{low} = V_{high} = 0$. A finite current flow is calculated in the nonequilibrium situation of the device, which is established by including an electric dipole interaction term as a perturbation to the Hamiltonian in the active scattering region. A small thermal smearing term, k_BT (=0.026 eV), is subtracted from μ_1 and added to μ_2 to take into account the electronic temperature at the interfaces in the nonequilibrium condition.

III. RESULTS AND DISCUSSION

A. $I-V$ for Different Junction Geometries. The calculated current−voltage characteristics for different junction geometries are presented in Figure 1. Several intriguing features are noticeable. First, in the case of the ONTOP junction geometry at both interfaces (Figure 1a), a sharp increase in current is observed after a V_{th} for all distances. A closer examination reveals a very small shift in V_{th} toward a higher value when d changes from 2.42 Å to 2.62 Å. It should be noted that 2.42 Å is the equilibrium S−Au interfacial distance. We have varied the S−Au interfacial distances and compared the total energy for various distances to find the equilibrium configuration. However, as we approach the weakly coupled regime by increasing d further, V_{th} is found to shift toward a lower value, which suggests that the value for V_{th} depends nonlinearly on the interfacial distance. For higher bias beyond V_{th}, a current plateau (ON state) is observed; the width of the current plateau is found to increase with the increase of d. The current remains relatively small and flat (OFF state) prior to V_{th}. Experimental measurement in a ruthenium−bis-(terpyridine) complex reported[16] a similar $I-V$ feature with current switching at 1.7 ± 0.25 V. For the interfacial distances considered in our calculation, the value for V_{th} is found to vary within ∼1.5 V to ∼2.0 V. For d = 3.02 Å, our calculation yields a small negative differential resistance (NDR) feature in the current−voltage characteristic. When the molecule is rotated about the Z-axis by θ = 15° (Figure 1b), a sharp increase in current is observed after a V_{th} . Increasing the θ from 15° to 20°, the threshold value shifted from ∼1.75 V to ∼1.3 V, and a plateau is observed for higher bias beyond V_{th}, as observed for the weakly coupled case (Figure 1a).

For the HOLLOW binding sites at both interfaces (Figure 1c), the calculated current is found to increase steadily with applied bias for all interfacial distances that we have considered. Unlike the ONTOP junction geometry (Figure 1a), the magnitude of the current for the HOLLOW configuration is

dx.doi.org/10.1021/jp3043335 | J. Phys. Chem. C 2012, 116, 17268−17273

found to decrease for higher d over the bias range from 0 to 3 V. Comparing the magnitude of current between junction geometries with ONTOP and HOLLOW binding sites, a higher current is noted for the HOLLOW binding geometry. For example, for d = 2.82 Å, the ONTOP junction geometry yields a current value of 0.024 μA at 1.35 V in contrast to 2.910 μA for the HOLLOW junction geometry. When the molecule is rotated about the Z-axis (Figure 1d), we do not observe a current plateau in the $I-V$ curve as found in the weakly coupled junctions with an ONTOP binding site; the current is found to increase steadily with the increase in applied bias beyond V_{th}.

In the case of ONTOP junction geometry on one side and HOLLOW on the other (Figure 1e), as we approach the weakly coupled junction by increasing the interfacial distance, a current plateau in $I-V$ beyond V_{th} is observed. Rotation of the molecule about the Z-axis yields a similar feature in $I-V$ as observed in Figure 1b. These calculations thus confirm that the experimental measurements are most likely for a weakly coupled junction with an ONTOP junction geometry at one or both of the S–Au interfaces. It should be noted that though the $I-V$ feature obtained with the ONTOP junction geometry in a weakly coupled configuration agrees reasonably well with the experimental data, there is a 3 orders of magnitude difference in current between theory and experiment; our calculated current value is found to be of the order ~μA as compared to the ~nA reported from the experiment.[16] The discrepancy in the magnitude of current between theory and experiment can be understood as follows. First, the junction considered in the experiment could be much more weakly coupled than the one considered here. Second, our calculation is based on a static exchange correlation potential instead of a true dynamically corrected exchange correlation potential;[31−34] the use of a static exchange correlation potential is found to overestimate the magnitude of the current.

B. Conformational Change. To see if the conformational change in the molecule between the lead causes switching in conductance, we recalculated the current for the ONTOP junction geometry (d = 2.42 Å) at both interfaces (Figure 2) by rotating one of the terpyridine planes from its equilibrium configuration by an angle Φ. It should be noted that, for the equilibrium structure, the two terpyridine planes are almost perpendicular to each other. We found the current remains relatively flat for bias up to ~2 V and switches to a higher conductance state for higher bias beyond ~2 V. A very similar feature in $I-V$ was noted for d = 2.42 Å with the ONTOP junction geometry (Figure 1a). To examine if the conformational change considered here is achievable by thermal fluctuation, we calculated the energy difference between extended systems with Φ = 0° (equilibrium structure) and Φ = 10°, which is found to be 0.21 eV. This suggests that such a conformational change may not be possible by thermal fluctuation. This study thus rules out that the switching behavior in conductance observed in the experiment is due to conformational change. Comparing the magnitude of current (Figure 1a and Figure 2), we observed a higher magnitude of current after the threshold bias for the molecule with conformational change. Conformational change makes the two terpyridine rings closer to a planar configuration, allowing the electron to delocalize between the two rings, resulting a higher current.[35]

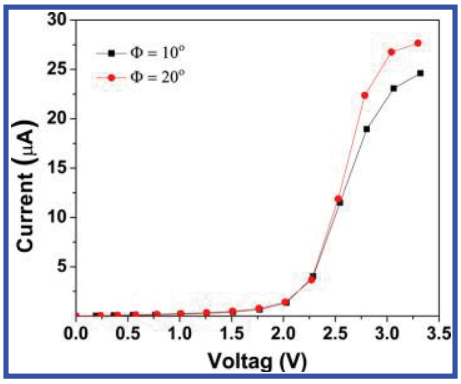

Figure 2. Current–voltage characteristics for Ru–bis(terpyridine) molecular wire with two different conformations of the molecular spacer; Φ represents the angle of rotation for one terpyridine plane from its equilibrium configuration about the current-flow axis.

C. Transmission. To understand the origin of the switching behavior of the current, we look into the bias dependent transmission function. The chemical potential window (CPW) is shown by the dotted lines, and the Fermi energy is set to zero in the energy scale. The area under the transmission curve between the CPW determines the current. Since the $I-V$ feature for the junction with the ONTOP binding site compares reasonably well with the experimental $I-V$ feature, we have presented the bias dependent transmission function for the ONTOP junction geometry. For brevity, we have only plotted bias dependent transmission (Figure 3) for d = 2.42 Å, 2.82 Å, and 3.02 Å, respectively. Several points are noticeable. First, in all cases, the transmission peaks shift toward the right with the increase in applied bias. In the case of a strongly coupled junction (Figure 3a), the transmission peaks are outside the CPW for V = 0.985 and 2.014 V. This is the reason we do not observe any significant change in current by increasing bias up to ~2 V; the current remains relatively small and flat. Increasing the bias further, for V = 3.050 V, the chemical potential window encloses transmission peaks at E = −1.07 eV and E = 1.38 eV, resulting in a sudden increase in current. Increasing the bias from V = 3.050 to 3.443 V, the window width for CPW increases, and an additional transmission peak at E = 1.68 eV appears within the window; this results in a higher current for V = 3.443 V than that for V = 3.050 V.

In the case of d = 2.82 Å (Figure 3b), for V = 0.953 V, no transmission peaks appear within the CPW. As we increase the bias to 2.305 V, the transmission peaks at ~ −0.85 eV appear within the CPW, resulting in a sudden increase in current. Though the CPW width increases by increasing the bias from 2.305 to 2.710 V, no additional transmission peaks appear within the CPW, resulting in a current plateau as shown in Figure 1a. For V = 3.523 V, the transmission peak at 1.63 eV that appears within the CPW leads to an increase in current. In the case of a weakly coupled junction (d = 3.02 Å), as expected, the transmission peaks are much sharper. For V = 1.075 V, no transmission peaks are included within the CPW. As we increase the bias to 1.901 V, the transmission peaks at ~ −0.65 eV appear within the CPW. No additional peaks appear within the CPW by increasing the bias to 3.140 V. A close look at the height of the transmission peak within the CPW for V = 1.901 and 3.140 V reveals the transmission peak height to decrease slightly in the case of V = 3.140 V. This leads to a smaller current for V = 3.140 V as compared to V = 1.901 V, resulting in a slope change in the $I-V$ leading to NDR. A similar observation was noted for the transmission in the Fe–

dx.doi.org/10.1021/jp3043335 | J. Phys. Chem. C 2012, 116, 17268–17273

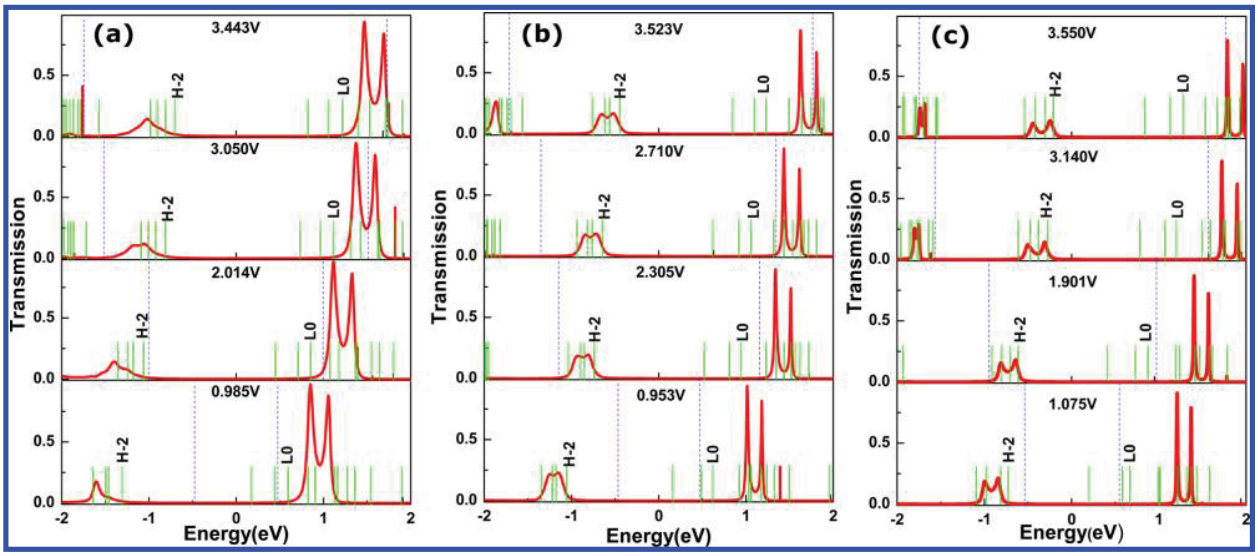

Figure 3. Bias dependent transmission as a function of injection energy for interfacial distancess of (a) 2.42 Å, (b) 2.82 Å, and (c) 3.02 Å, respectively. The Fermi energy is set to zero in the energy scale; the dotted lines in each panel represent the chemical potential window. The eigen channels of the extended molecule are shown by solid vertical lines; L0 and H-2 refer to LUMO and HOMO-2, respectively.

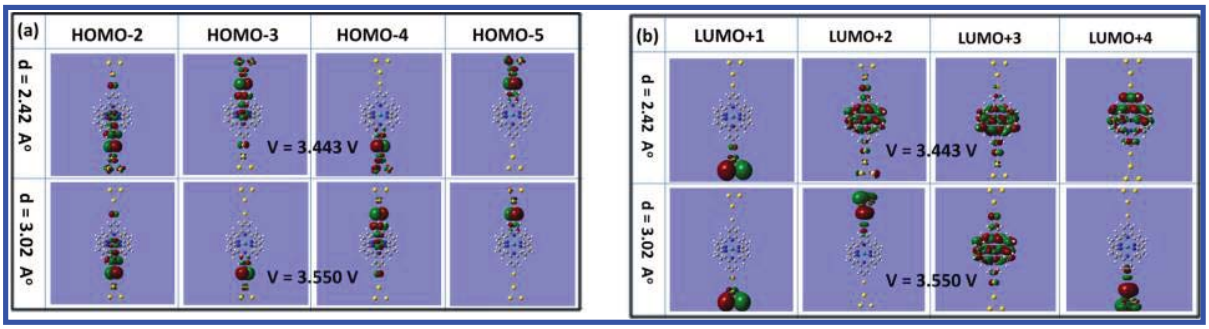

Figure 4. Participating bias dependent (a) occupied and (b) unoccupied molecular orbitals for strongly coupled (d = 2.42 Å) and weakly coupled (d = 3.02 Å) junctions. HOMO and LUMO refer to highest occupied molecular orbital and lowest unoccupied molecular orbital, respectively.

terpyridine molecular junction.[20] A part of the transmission peak at 1.73 eV is included within the CPW for V = 3.550 V, resulting in a higher current for V = 3.550 V. When we compared the transmission for three different d values, a shift in the transmission peak position toward a higher energy value is observed for a higher d.

Further inspection of Figure 3 reveals that the threshold bias in a strongly coupled junction is dictated by the transmission peaks from the unoccupied states. In contrast, for a weakly coupled junction, the threshold bias value is dictated by the transmission peaks from the occupied states. For a deeper understanding, we analyze the eigen-channels that contribute to the transmission. In the case of a strongly coupled junction (d = 2.42 Å), LUMO+1, LUMO+2, and LUMO+3 contribute to the transmission peaks at 0.85 and 1.05 eV for V = 0.985 V. The LUMO+1 has s-orbital character of Au; LUMO+2 and LUMO +3 have s-character of gold, d-character of Ru, and p-character of neighboring N and C atoms that connect to Ru. For higher bias (V = 3.443 V), no significant change in the orbital character is noticed (Figure 4a). HOMO-2, HOMO-3, HOMO-4, and HOMO-5 contribute to the broadened transmission peak at −1.60 eV for V = 0.985 V. HOMO-2 and HOMO-3 have d-character of Ru and d-character of Au together with the p-character of N, C, and S. HOMO-4 and HOMO-5 have s- and p-characters of C, p-character of S, and d-character of Au. In the case of a weakly coupled junction, the same set of orbitals contribute to the transmission. The orbital character analysis indicates no contribution from Au for HOMO-2, HOMO-3, HOMO-4, and HOMO-5 (Figure 4a); in the weakly coupled junction, LUMO+1 and LUMO+2 have s-character for Au and S, and LUMO+3 has almost no contribution from Au (Figure 4b). The contribution from the s-orbital of Au to the transmission leads to a more sudden increase of current in a strongly coupled junction than that in the weakly coupled junction. Thus, this orbital analysis provides an explanation for the observed higher current after the threshold bias in a strongly coupled junction as compared to the weakly coupled junction; the much higher current in the strongly coupled junction is due to metal(Au) dominated states.

IV. CONCLUSIONS

We present a first principles calculation of current−voltage characteristics in a Ru−bis(terpyridine) molecular junction, which has been fabricated and characterized using STM. An ensemble of prototypical device structures is constructed by varying metal−molecule binding site, interfacial distance, orientation of the molecule at the interface, and conformational change in the molecule to study junction dependent conductance. A bias dependent Green's function approach in

dx.doi.org/10.1021/jp3043335 | J. Phys. Chem. C 2012, 116, 17268−17273

conjunction with an orbital dependent DFT is used to study the $I-V$ characteristics. Comparison of calculated $I-V$ with the experimental data allows us to identify the possible atomic level structural details of the metal−molecule interface in the experimental measurement; the weakly coupled ONTOP junction geometry is found to yield a $I-V$ curve with a switching feature that agrees reasonably well with the experimental result. Analysis of the bias dependent transmission and the orbital character of the participating eigen-channel is presented to explain the origin of distinct $I-V$ features observed in strongly and weakly coupled junction geometries. In the weakly coupled junction, occupied orbitals having d-character of Ru and p-characters of S, C, and N in the molecular interconnect are found to dictate the switching behavior in $I-V$. In contrast, in the strongly coupled junction, the unoccupied gold dominated states dictate the sudden increase of current at a threshold bias. Thus, this study provides an electronic structure level explanation of the observed switching behavior in the Ru−bis(terpyridine) molecular junction.

AUTHOR INFORMATION

Corresponding Author

*E-mail: patir@mtu.edu. Phone: 906-487-3193. Fax: 906-487-2933.

Notes

The authors declare no competing financial interest.

ACKNOWLEDGMENTS

This work is supported by the NSF through Grant No. 0643420.

REFERENCES

(1) Aviram, A.; Ratner, M. A. *Chem. Phys. Lett.* **1974**, *29*, 277−283.
(2) Donhauser, Z. J.; Mantooth, B. A.; Kelly, K. F.; Bumm, L. A.; Monnell, J. D.; Stapleton, J. J.; Price, D. W., Jr.; Rawlett, A. M.; Allara, D. L.; Tour, J. M.; Weiss, P. S. *Science* **2001**, *292*, 2303−2307.
(3) Reed, M. A.; Zhou, C.; Muller, C. J.; Burgin, T. P.; Tour, J. M. *Science* **1997**, *278*, 252−254.
(4) Zhou, J.; Chen, F.; Xu, B. *J. Am. Chem. Soc.* **2009**, *131*, 10439−10446.
(5) Hihath, J.; Bruot, C.; Nakamura, H.; Asai, Y.; Dez-Perez, I.; Lee, Y.; Yu, L.; Tao, N. *ACS Nano* **2011**, *5*, 8331−8339.
(6) Nitzan, A.; Ratner, M. A. *Science* **2003**, *300*, 1384−1389.
(7) Tao, N. J. *Nat. Nanotechnol.* **2006**, *1*, 173−181.
(8) Xu, B.; Tao, N. J. *Science* **2003**, *301*, 1221−1223.
(9) Cui, X. D.; Primak, A.; Zarate, X.; Tomfohr, J; O. F. Sankey, O. F.; Moore, A. L.; Moore, T. A.; Gust, D.; Harris, G.; Lindsay, S. M. *Science* **2001**, *294*, 571−574.
(10) Huang, Z.; Chen, F.; Bennett, P. A.; Tao, N. *J. Am. Chem. Soc.* **2007**, *129*, 13225−13231.
(11) Hu, Y.; Zhu, Y.; Guo, H. *Phys. Rev. Lett.* **2005**, *95*, No. 156803(1−4).
(12) French, W. R.; Lacovella, C. R.; Cummings, P. T. *ACS Nano* **2012**, *6*, 2779−2789.
(13) Pontes, R. B.; Rocha, A. R.; Sanvito, S.; Fazzio, A.; Silva, A. J. R. *ACS Nano* **2011**, *5*, 795−804.
(14) Andrews, D. Q.; Van Duyne, R. P.; Ratner, M. A. *Nano Lett.* **2008**, *8*, 1120−1126.
(15) Zhou, J. G.; Hagelberg, F. *Phys. Rev. Lett.* **2006**, *97*, No. 045505(1−4).
(16) Seo, K.; Konchenko, A. V.; Lee, J.; Bang, G. S.; Lee, H. *J. Am. Chem. Soc.* **2008**, *130*, 2553−2559.
(17) Datta, S. *Electron Transport in Mesoscopic Systems*; Cambridge University Press: Cambridge, U.K., 1997.
(18) Di Ventra, M. *Electrical Transport in Nanoscale Systems*; Cambridge: New York, 2008.
(19) Taylor, J.; Guo, H.; Wang, J. *Phys. Rev. B* **2001**, *63*, No. 245407(1−13).
(20) Pati, R.; McClain, M.; Bandyopadhyay, A. *Phys. Rev. Lett.* **2008**, *100*, No. 246801(1−4).
(21) C. Toher, C.; Sanvito, S. *Phys. Rev. Lett.* **2008**, *99*, No. 056801(1−4).
(22) Brandbyge, M.; Mozos, J. L.; Ordejon, P.; Taylor, J.; Stokbro, K. *Phys. Rev. B* **2002**, *65*, No. 165401(1−17).
(23) Xue, Y.; Datta, S.; Ratner, M. A. *J. Chem. Phys.* **2001**, *115*, 4292−4299.
(24) Su, W.; Jiang, J.; Lu, W.; Luo, Y. *Nano Lett.* **2006**, *6*, 2091−2094.
(25) Solomon, G. C.; Herrmann, C.; Hansen, T.; Mujica, V.; Ratner, M. A. *Nat. Chem.* **2010**, *2*, 223−228.
(26) Mandal, S.; Pati, R. *Phys. Rev. B* **2011**, *84*, No. 115306(1−5).
(27) Pal, P. P.; Pati, R. *Phys. Rev. B* **2010**, *82*, No. 045424(1−6).
(28) Parr, R. G.; Yang, W. *Density-Functional Theory of Atoms and Molecules*; Oxford Science: Oxford, 1994.
(29) *GAUSSIAN 03*; Gaussian Inc.: Pittsburgh, PA, 2003.
(30) Becke, A. D. *J. Chem. Phys.* **1993**, *98*, 5648−5652.
(31) Runge, E.; Gross, E. K. U. *Phys. Rev. Lett.* **1984**, *52*, 997−1000.
(32) Evers, F.; Weigend, F.; Koentopp, M. *Phys. Rev. B* **2004**, *69*, No. 235411(1−9).
(33) N. Sai, N.; Zwolak, M.; Vignale, G.; Di Ventra, M. *Phys. Rev. Lett.* **2005**, *94*, No. 186810(1−4).
(34) Vignale, G.; Di Ventra, M. *Phys. Rev. B* **2009**, *79*, No. 014201(1−10).
(35) Pati, R.; Karna, S. P. *Phys. Rev. B* **2004**, *69*, No. 155419(1−5).